Title

Crystallization behavior of a gas atomized Al85Ni10La5 amorphous alloy

Journal

Journal of Non-Crystalline Solids, 351(19-20)

ISSN

0022-3093

Authors

Zhang, Zhihui

Witkin, D

Lavernia, E J

Publication Date

2005-07-01

Peer reviewed

Available online at www.sciencedirect.com
SCIENCE DIRECT®
Journal of Non-Crystalline Solids xxx (2005) xxx–xxx
JOURNAL OF NON-CRYSTALLINE SOLIDS
www.elsevier.com/locate/jnoncrysol

Crystallization behavior of a gas atomized $Al_{85}Ni_{10}La_5$ amorphous alloy

Zhihui Zhang [a,*], David Witkin [b], Enrique J. Lavernia [a]

[a] Department of Chemical Engineering and Materials Science, University of California, Davis, CA 95616, United States
[b] Department of Chemical Engineering and Materials Science, University of California, Irvine, CA 92697, United States

Received 19 August 2004; received in revised form 5 April 2005

Abstract

$Al_{85}Ni_{10}La_5$ (at.%) alloy powders were fabricated using gas atomization. X-ray diffraction analysis revealed that powders in the size range of <500 mesh (<25 μm) are amorphous. The crystallization behavior and kinetics of the amorphous $Al_{85}Ni_{10}La_5$ powders (<25 μm) were investigated during continuous heating and isothermal annealing. The amorphous $Al_{85}Ni_{10}La_5$ alloy undergoes a multi-step crystallization reaction in the temperature range of 250–390 °C. The activation energies for the first exothermic reactions were determined as 344 kJ/mol. Instead of a primary crystallization, a eutectic reaction was found to be associated with the first reactions and the crystalline phases were identified as fcc-Al, $Al_{11}La_3$, Al_3Ni and a metastable phase Al_3La. The isothermal annealing was carried out at temperatures of 235 °C, 245 °C and 250 °C. Results from the isothermal annealing analyses revealed presence of quenched-in Al nuclei. The influence of isothermal annealing on the thermal stability of the $Al_{85}Ni_{10}La_5$ powders (<25 μm) is also discussed.

IDT: A180; C290

PACS: 61.43.Dq; 61.46.+w; 64.70.Kb

1. Introduction

Interest in the study of high-strength and light-weight materials has intensified in recent years, partly due to rising energy costs. For aluminum alloys, an upper tensile strength in the range of 550–600 MPa may be readily achieved via age hardening, and usually does not exceed 700 MPa even when invoking other strengthening approaches, such as Hall–Petch strengthening, solid solution hardening, and dispersion strengthening [1]. The theoretical shear strength for Al free of defects is estimated as around 1500 MPa [2]. However, since the Al-rich amorphous alloy family of Al–R–TM (R-rare earth metal, TM-transition metal) was discovered [3,4], it has been suggested that the tensile strength may reach as much as 1500 MPa if this type of amorphous alloy is partially devitrified and contains a microstructure consisting of both nanocrystalline and amorphous phases [5]. The dimensions of Al–R–TM amorphous alloys, however, are currently limited to rapidly solidified powders or ribbons. Thus increasing efforts have been focused on producing bulk forms that retain a nanocrystalline/amorphous microstructure after subsequent compaction and consolidation of the amorphous precursors (gas-atomized powders and melt-spun ribbons, etc.) [5–7]. A clear understanding of their thermal stability and the crystallization behavior is necessary to control the compaction processes and achieve good mechanical properties as well as microstructures, espe-

* Corresponding author. Tel.: +1 530 297 7251.
E-mail address: zhizhang@ucdavis.edu (Z. Zhang).

0022-3093/$ - see front matter © 2005 Published by Elsevier B.V.
doi:10.1016/j.jnoncrysol.2005.04.055

cially for controlling the precipitation of nanocrystalline aluminum crystallites, which are regarded as a likely source of the high strength for the alloys [2,5]. Precipitation of intermetallic compounds could further harden this alloy, but it is anticipated that they will diminish the ductility [8]. In the current study, the crystallization of an alloy with the atomic composition of $Al_{85}Ni_{10}La_5$ is studied with particular attention to precipitation of the Al phase.

2. Experimental

The amorphous aluminum alloy powders used in the present investigation were prepared by gas atomization. A mixture of pure elemental Al (99.99 wt%), Ni (99.9 wt%) and La (99.9 wt%) with the nominal chemical composition of $Al_{85}Ni_{10}La_5$ (at.%) was induction melted under a high-purity Ar atmosphere and then atomized at a superheat level of approximately 250 °C using high-purity He gas with an atomizing pressure of 6.2 MPa. The powders were mechanically sieved at mesh sizes 500 (25 μm) and 270 (53 μm). X-ray diffraction analysis (XRD) showed that particles between 25 μm and 53 μm diameter were partially amorphous whereas particles less than 25 μm were essentially amorphous, as seen in Fig. 1(a). The amorphous nature of the $Al_{85}Ni_{10}La_5$ powders less than 25 μm was further confirmed by transmission electron microscopy (TEM), shown in Fig. 1(b), although crystalline phases might be found in certain particles which, for whatever reason during the atomization process, had experienced a slower cooling history.

On the basis of these results, the atomized powders less than 25 μm were examined by means of differential scanning calorimetry (DSC) in terms of continuous heating and isothermal annealing processes. DSC was carried out on a Perkin–Elmer DSC-7 using ultra-high purity N_2 as the purging gas. The XRD analyses were carried out with a Scintag XDS 2000 X-ray diffractometer using CuK_α radiation. TEM was carried out using a Philips CM-12 electron microscope operating at 100 kV. Additional microscopic characterization of cross-sections of the devitrified powders was examined using a XL 30 FEG scanning electron microscope (SEM) (Fig. 2).

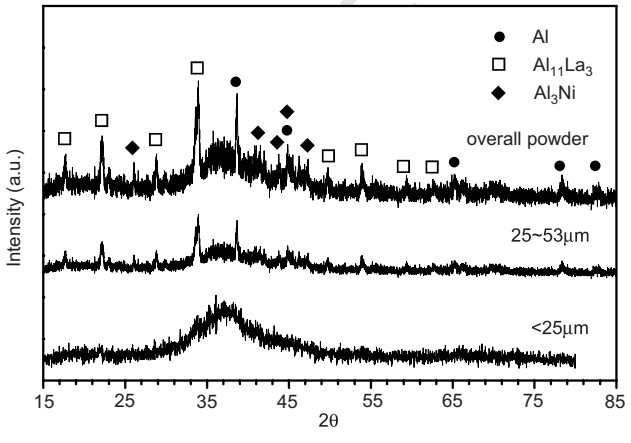

Fig. 1. XRD patterns of gas atomized $Al_{85}Ni_{10}La_5$ powders.

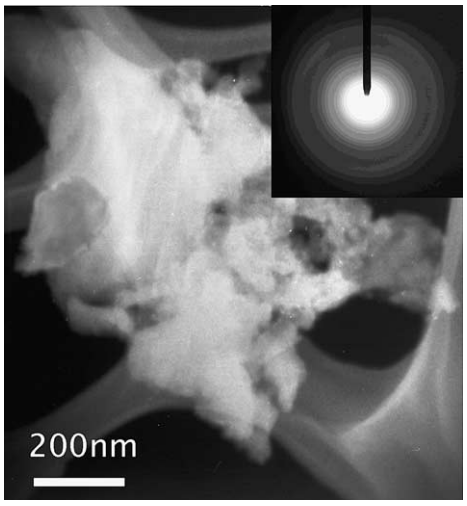

Fig. 2. TEM dark field micrograph and selected area diffraction pattern of amorphous $Al_{85}Ni_{10}La_5$ powders (<25 μm).

3. Results

Fig. 3 shows the continuous heating DSC traces of the $Al_{85}Ni_{10}La_5$ amorphous powders (<25 μm) using heating rates from 2.5 °C/min to 40 °C/min. Crystallization processes occurred between 250 °C and 390 °C. Three distinct exothermic peaks were observed during the devitrification process. At high heating rates (>20 °C/min), a minor endothermic signal, indicating

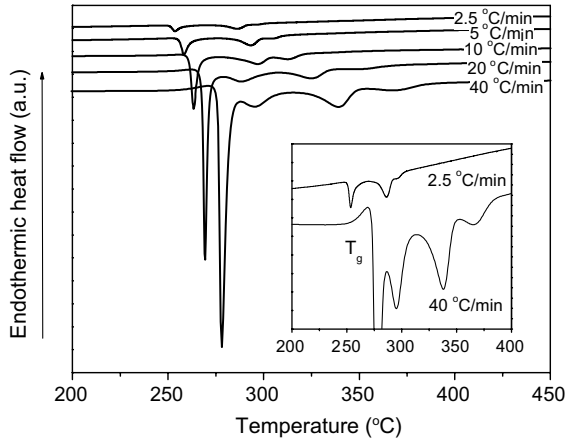

Fig. 3. Continuous heating DSC traces of $Al_{85}Ni_{10}La_5$ amorphous powders (<25 μm). The inset picture shows the enlarged curves for the heating rate of 40 °C /min and 2.5 °C/min.

the glass transition, was observed prior to the first crystallization peak, while another minor exothermic peak was found after the third exothermic peak. At low heating rates (<5 °C/min), the endothermic peak for glass transition was not resolved due to the fact that it overlapped with the subsequent exothermic peak. In order to determine the crystallized phase corresponding to the first exothermic peak, the amorphous powders were heated to the peak temperature of 263 °C at a heating rate of 10 °C/min and held for 5 min. The heat-treated powders were then analyzed using XRD. The XRD results showed the first exothermic peak corresponded to a eutectic-like reaction [9]:

$$\text{amorphous} \rightarrow \text{amorphous} + \text{Al} + \text{Al}_3\text{Ni} + \text{Al}_{11}\text{La}_3 + \text{Al}_3\text{La (metastable)}$$

The precipitated phases consisted of three equilibrium phases: Al, Al_3Ni, $Al_{11}La_3$ and a metastable phase Al_3La. XRD analysis of amorphous powders that were heated to 500 °C indicated that the fully crystallized phases consisted only of Al, Al_3Ni and $Al_{11}La_3$; the metastable phase Al_3La had disappeared. In other words, the phase composition of the fully crystallized powder is the same as that of the coarse powders larger than 25 μm.

In related studies [10–12], however, the first devitrification peak occured in terms of the primary crystallization of fcc-Al and the activation energy for this reaction was found to be close to the self-diffusion activation energy of Al (144.2 kJ/mol). The apparent activation energy controlling an exothermic reaction can be determined by the Kissinger method [13].

$$\ln\left(\frac{v}{T^2}\right) = -\frac{E_a}{RT} + C,$$

where v is the heating rate, R is the gas constant, T is the characteristic temperature and can be frequently selected as the peak temperature T_p or the onset temperature T_{on}. The term C is a constant ($C = Rk_0/E_a$, where k_0 is the pre-exponential factor in the Arrhenius equation $k = k_0\exp(-E_a/RT)$). The respective activation energies are then determined from the slope of the curves $\ln(v/T_p^2)$ vs. $1/T_p$. The crystallization onset temperatures and the peak temperatures for the first three peaks determined by DSC tracing are listed in Table 1. The plots of $\ln(v/T_p^2)$ vs. $1/T_p$ are given in Fig. 4. The activation energies corresponding the first peaks and the third peaks are linearly fitted to be 344 kJ/mol and 198 kJ/mol, respectively. Again, the activation energy determination supported the conclusion that the first peak underwent a reaction other than the precipitation of fcc-Al. The second peaks do not exhibit a linear relationship and it is probably because the reactions are sensitive to temperatures and thus the activation energies are temperature dependent.

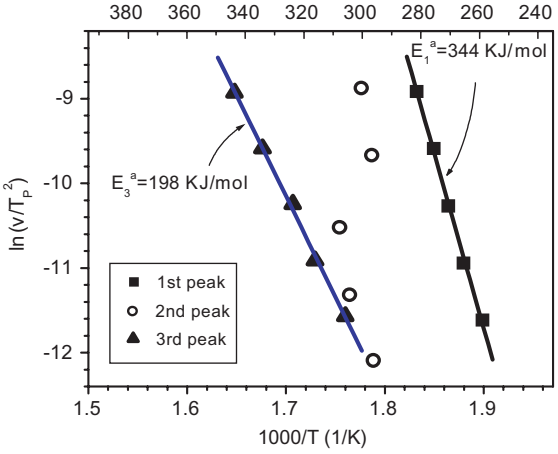

Fig. 4. Kissinger plots of gas atomized $Al_{85}Ni_{10}La_5$ powders.

Precipitation of nanosized fcc-Al phase is favored because the amorphous $Al_{85}Ni_{10}La_5$ alloy will be further hardened due to dispersions of nanoscale Al crystallites [5] as well as the solute concentration enrichment in the amorphous matrix [14]. Precipitation of intermetallic compounds could further increase the hardness but is anticipated to decrease the ductility of this alloy [8]. As a result, it is necessary to examine the conditions that might promote the precipitation of fcc-Al and retard the occurrence of intermetallic compounds. To investigate these possible conditions, the amorphous $Al_{85}Ni_{10}La_5$ alloy powders were subjected to isothermal annealing below the glass transition temperature.

Isothermal DSC traces of the $Al_{85}Ni_{10}La_5$ amorphous powders are shown in Fig. 5. The samples were heated to temperatures of 235 °C, 245 °C and 250 °C, respectively, at a heating rate of 200 °C/min and held

Table 1
Onset and peak temperatures of the exothermic reactions at various heating rates

Heating rate (°C/min)	First peak		Second peak		Third peak	
	Onset (°C)	Peak (°C)	Onset (°C)	Peak (°C)	Onset (°C)	Peak (°C)
2.5	249.8	253.6	269.3	286.2	–	295.2
5	253.1	259.0	276.6	293.8	298.3	305.3
10	258.8	263.4	276.7	297.0	304.7	312.9
20	264.6	267.6	276.8	286.6	306.4	323.6
40	268.5	272.8	282.9	290.0	310.9	333.8

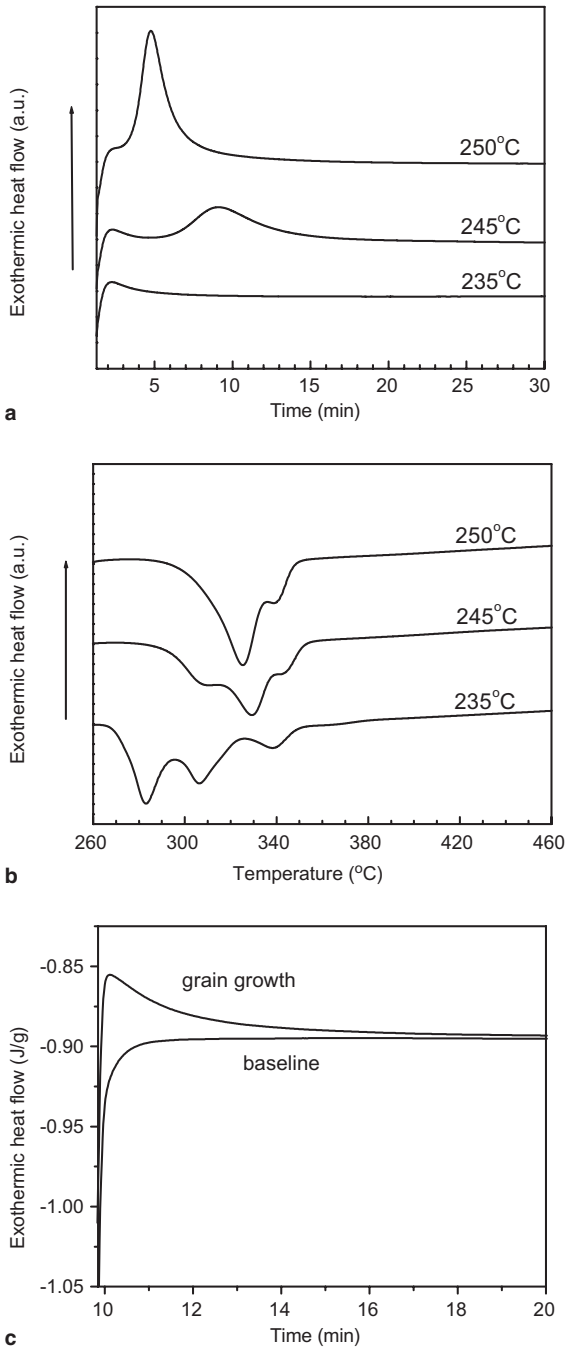

Fig. 5. Isothermal annealing of $Al_{85}Ni_{10}La_5$ amorphous powders (<25 μm) at 235 °C, 245 °C and 250 °C (a). Continuous heating traces of the powders annealed at 235 °C, 245 °C and 250 °C (b). Isothermal tracing at 235 °C showing a monotonically decreasing signal (c).

for 30 min (Fig. 5(a)), followed by continuous heating to 500 °C at a rate of 40 °C/min (Fig. 5(b)). The holding temperature 250 °C was selected on the basis of the onset temperature of the first crystallization peak at a slow heating rate (2.5 °C/min). Exothermic bell-shaped peaks occurred in the isothermal curves at 245 °C and 250 °C and the exothermic peaks overlapped in the subsequent continuous DSC tracing from the holding temperature to 500 °C. However, a monotonically decreasing signal was observed in the isothermal DSC curve of 235 °C and the three distinct exothermic peaks were clearly resolved in the subsequent continuous temperature scan. In order to rule out that the signal may have been the result of an instrumental artifact due to heat flow overshoot, a quality-assurance test was completed using a heating rate of 20 °C/min, followed by re-running the temperature program with the transformed sample after it had cooled to room temperature, as shown in Fig. 5(c). The baseline signal gave a perfect horizontal line indicating that the monotonically decreasing signal resulted from phase transformation in the sample. Therefore the $Al_{85}Ni_{10}La_5$ amorphous alloy showed different crystallization behavior during holding at 235 °C from above 245 °C.

The transformation process during the isothermal ageing was further analyzed using the Johnson–Mehl–Avrami (JMA) phenomenological model [15]:

$$\zeta = 1 - \exp(-k(t-\tau)^n),$$

where ζ is the transformed volume fraction, n is the Avrami exponent which depends on the transformation mechanism, and τ is the incubation time at which a region nucleates. The term k is the reaction constant.

An isothermal calorimetry signal showing a monotonically decreasing curve is evidence of growth from pre-existing nuclei, and leads to an Avrami exponent n that is less than 1. In contrast, the presence of a peak suggests a nucleation and growth process where the Avrami exponent n turns out to be greater than 1 [16]. The specific value of n can be obtained by fitting the curves of transformed volume fractions vs. the annealing time. As shown in Fig. 6(a) and (b), when the $Al_{85}Ni_{10}La_5$ amorphous alloy was annealed at 235 °C, the data from Fig. 5(c) was fitted to the JMA equation, giving an Avrami exponent equal to 0.87. For annealing at 245 °C and 250 °C, the transformed volume fractions calculated from Fig. 5(a) are shown in Fig. 6(a) and the Avrami plots of $\ln(-\ln(1-\zeta))$ vs. $\ln(t)$ are given in Fig. 6(b). The Avrami exponents at 245 °C are equal to 3.3 at the initial stage and then decrease to 1.9 at the final stage. In the case of 250 °C, the Avrami exponent starts at 3.9 before finally decreasing to 1.7. The non-linear nature of the Avrami plots implies that the transformation mechanisms have changed in the final crystallization stage. The XRD patterns for the samples annealed at 235 °C, 245 °C and 250 °C are shown in Fig. 7. It is observed that only precipitation of the fcc-Al phase occurred at 235 °C. At 245 °C, the Al phase and intermetallic compounds $Al_{11}La_3$, Al_3Ni and Al_3La formed in a eutectic-like reaction. The phases formed during annealing at 250 °C were apparently similar to those observed at 245 °C. For comparison, the XRD pattern for the powders that were annealed at 283 °C

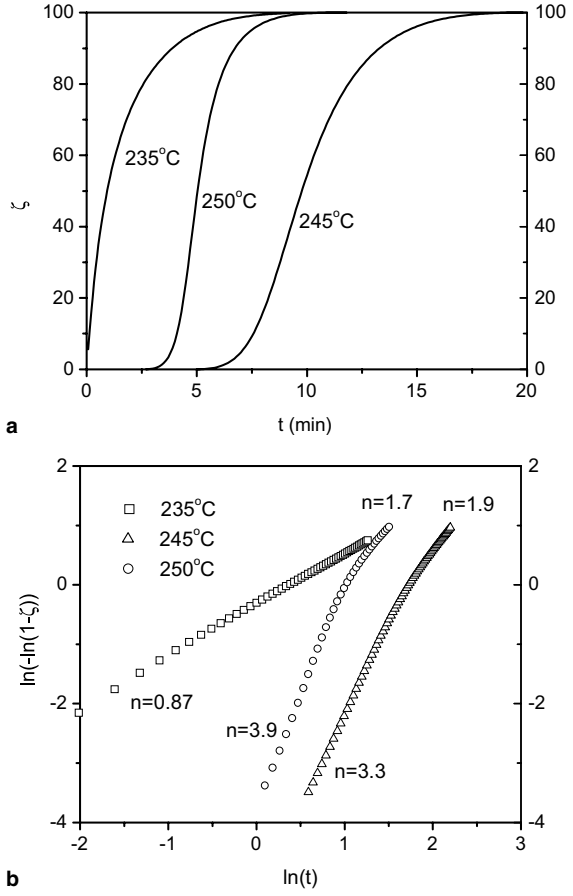

Fig. 6. Plots of transformed volume fraction vs. annealing time (a) and the Avrami plots (b).

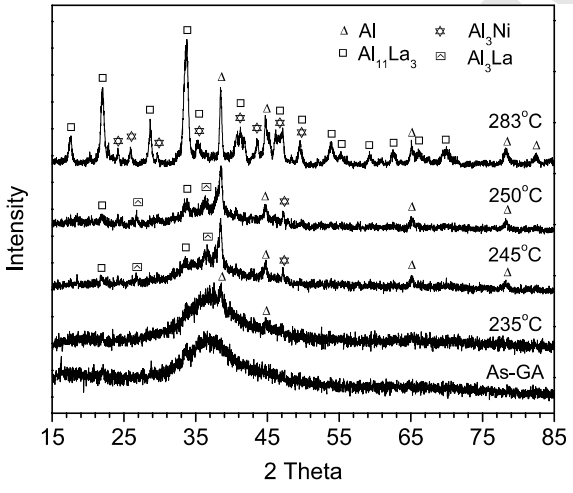

Fig. 7. XRD patterns of $Al_{85}Ni_{10}La_5$ powders (<25 μm) annealed at various temperatures compared to the as-atomized (GA) powders.

for 5 min is also plotted in Fig. 7. It can be seen that the metastable phase Al_3La has disappeared under the annealing condition.

4. Discussion

The present results show that amorphous $Al_{85}Ni_{10}La_5$ powders can be produced by gas atomization, at least under the experimental conditions used herein. The intermetallic phases do not precipitate, even as the matrix is heated up to an annealing temperature of 235 °C. The observation of a monotonically decreasing signal during the isothermal DSC tracing performed at 235 °C suggests a growth reaction [16,17], indicating the presence of quenched-in nuclei in the amorphous matrix. As seen in Fig. 7, only fcc-Al phase was detected after annealing at 235 °C. In contrast, observation of an exothermic peak suggested a nucleation and growth reaction during isothermal annealing at 245 °C and 250 °C. This divergence in devitrification behavior was in agreement with the subsequent continuous DSC scans following the isothermal annealing. As shown in Fig. 5(b), the three exothermic reactions, which can be seen in the continuous heating curves (Fig. 3), are well-defined in the powders annealed at 235 °C but could not be resolved any more in the powders annealed at 245 °C and 250 °C. It suggests that the exothermic peaks in Fig. 5(a) are those missing first peaks in Fig. 5(b). The reaction products also support this suggestion. The crystalline phases (i.e., Al, $Al_{11}La_3$, Al_3Ni and Al_3La) formed at 245 °C and 250 °C are the same as those formed at the peak temperature 263 °C.

At a temperature of 245 °C, the Avrami exponent is 3.3 at the initial stage, followed by a decrease to 1.9. At 250 °C, the Avrami exponent is 3.9 at the initial stage and decreases to 1.7 in the late stage. The value of Avrami exponents between 3 and 4 has been interpreted as interface-controlled growth of nuclei with decreasing nucleation rate, while Avrami exponents in the range of 1.5 to 2.5 correspond to diffusion-controlled growth with a decreasing nucleation rate [15]. In the early stages, if assumptions of spatially randomly distributed nuclei are made, two typical cases can be considered: an Avrami exponent of 3 implies zero nucleation rates and the Avrami exponent of 4.0 means constant nucleation rates [18]. It is implied that the nucleation sites are nearly saturated at 245 °C while nucleation rates are close to constant at 250 °C. As shown in Fig. 5(a), a longer incubation period was observed at 245 °C than at 250 °C. The presence of an apparent incubation period at 245 °C and 250 °C also indicated that the nuclei were newly created during the incubation period and different from the quenched-in nuclei observed at 235 °C. The assumption of random nucleation is supported by electron microscopic observation. Fig. 8(a) shows an SEM micrograph for the cross-section of the partially crystallized powders after annealing at 250 °C for 0.5 h. The back-scattered electron image exhibits a featureless surface, indicating the size of the crystalline particles is beyond the instrumental resolution and no

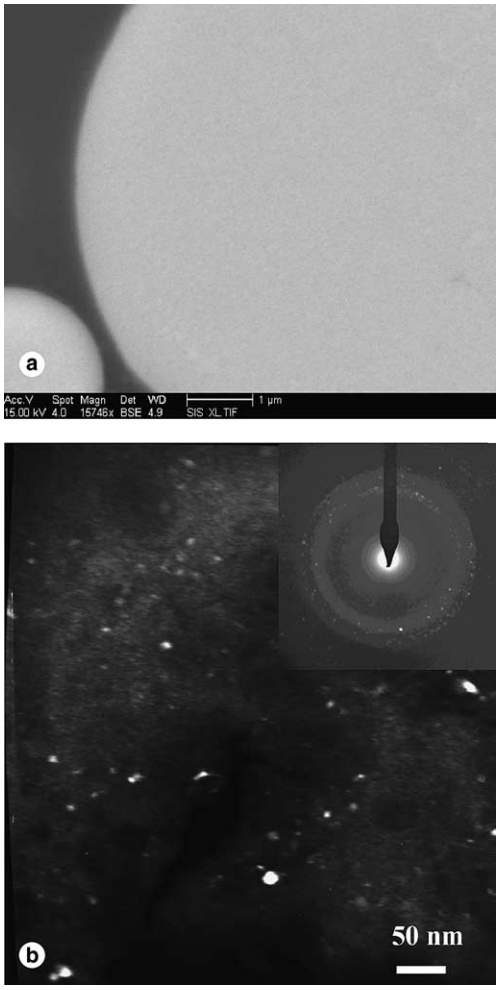

Fig. 8. Microstructures for the $Al_{85}Ni_{10}La_5$ powders (<25 μm) held at 250 °C. (a) SEM back-scattered electron image for the powder cross-section. (b) TEM dark field image and selected area diffraction pattern (inset).

particles larger than 100 nm are observed. Fig. 8(b) shows the TEM dark field image for powders subjected to the same thermal treatment. It can be seen that the size of the nanocrystallites is around 10–30 nm and they are randomly distributed in the amorphous matrix. During the later stages, the observed drop in the values of the Avrami exponent is perhaps attributed to the fact that growth of Al crystallite becomes dominant. As shown in Fig. 8(b), the SADP mainly comes from contribution of the Al crystallites. As the eutectic reaction occurs, precipitation of compounds will lead to depletion of La and Ni in the local areas. This will destabilize the amorphous matrix and induce diffusion of Al. As a result, diffusion-controlled growth of Al crystallites becomes more significant during the later stages.

For Al-based amorphous alloys, a primary crystallization of fcc-Al has often been suggested as the first transformation reaction [5,10–12,19]. In the case of Al–Ni–La alloys, the primary formation of fcc-Al was also observed in an $Al_{89}La_6Ni_5$ alloy [10] and an $Al_{88}La_6Ni_6$ alloy [12]. However, a eutectic reaction instead of a primary reaction corresponding to the first peak was recently identified in the same chemical composition of $Al_{89}La_6Ni_5$ [9]. In the current study, the first peaks in continuous DSC tracing correspond to a eutectic-like reaction associated with precipitation of the stable phase fcc-Al, Al_3Ni, $Al_{11}La_3$ and a metastable phase Al_3La. The XRD traces do not allow a simple identification of the phases precipitated during the second and the third peaks. By comparing the change of XRD peak intensities due to the second reactions, it implies that precipitation of the compounds also presents in the second reactions. The second peaks failed to fit the Kissinger equation and their positions changed abnormally with increasing heating rate. From Table 1 it can be seen that the onset temperatures for the second peaks were in the range of 269 °C to 283 °C. The Al_3La phase was not observed in the powders held at 283 °C for 5 min. Hence the second peak may be mainly related to formation of the La-rich phases. Studies of Al–Ni–Y and Al–Ni–Ce alloys suggested that the rare earth metals had lower mobility than Al as well as Ni [14]. Hence it is reasonable to assume that La also has lower mobility. It should be pointed out that the eutectic-like reaction requires long-range diffusion of La, the reaction however might not be simply diffusion-controlled and the rate-controlling mechanisms are sensitive to the temperatures. Hence the activation energy failed to attain a constant value, which could be attributed to a variation of the rate controlling mechanisms due to increasing temperature. Meanwhile a decrease of lanthanum concentration will destabilize the amorphous matrix and allow formation of the Al_3Ni phase.

It has been suggested that partially crystallizing an amorphous alloy with nanosized Al crystallites dispersed in the amorphous matrix would further enhance its mechanical properties and the Al phase would be obtained on basis of a primary crystallization reaction [2,5,8,20]. In the gas atomized $Al_{85}Ni_{10}La_5$ amorphous powders, quenched-in Al nuclei were found and the nanosized Al crystal could be developed by annealing the amorphous powders below the glass transition temperature. The size of the Al crystallite held at 235 °C for 0.5 h was around 5–20 nm based on TEM observations. It is noteworthy that precipitation of the elemental Al phase implies that the remnant amorphous phase becomes enriched with solute elements, especially near the aluminum crystals. These increased concentrations will stabilize the amorphous phase and impede crystallization [14,21]. Comparing Figs. 3 and 5(b), it can be seen that the first peak temperature shifted from 273 °C to 277 °C after the amorphous powder was held at 235 °C for 0.5 h. When we increased the ageing time from 0.5 h to 1 h, the peak shifted from 277 °C to 283 °C using the same heating rate of 40 °C/min, as

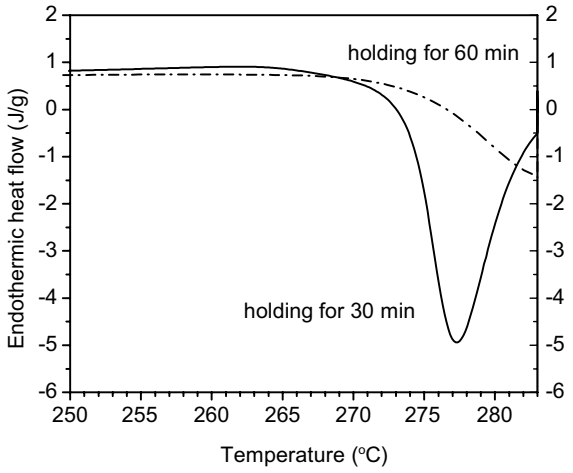

Fig. 9. Continuous DSC traces showing that the thermal stability can be improved by a pre-annealing at 235 °C.

shown in Fig. 9. This suggests that while nanoscale Al crystallites are being formed through growth the thermal stability of the amorphous phase has been increased.

5. Conclusions

(1) $Al_{85}Ni_{10}La_5$ powders were produced using gas atomization. The powder fraction with a particle size less than 25 μm was amorphous. The amorphous phase is stable during heating up to a temperature of 235 °C. An annealing treatment at this temperature could improve the thermal stability of the amorphous phase.

(2) Isothermal DSC traces indicate that quenched-in Al nuclei existed in the amorphous matrix. Transformation at 235 °C exhibited growth of aluminum nuclei. Crystallization above 245 °C exhibited a nucleation and growth process associated with a eutectic-like reaction. The eutectic-like reaction instead of a primary crystallization took place in the first exothermic peaks, during which fcc-Al phase was precipitated concurrently with intermetallic compounds of $Al_{11}La_3$ and Al_3Ni as well as a metastable phase Al_3La.

Acknowledgments

The authors would like to acknowledge the Army Research Office (Grant No. DAAD 19-03-1-0020 and Grant No. DAAD19-01-1-0627) for financial support. Particular thanks also go to Dr William Mullins for his support and assistance.

References

[1] J.-P. Immarigeon, R.T. Holt, A.K. Koul, L. Zhao, W. Wallace, J.C. Beddoes, Mater. Charact. 35 (1995) 41.
[2] H.S. Kim, P.J. Warren, B. Cantor, H.R. Lee, Nanostruct. Mater. 11 (1999) 241.
[3] Y.H. Kim, A. Inoue, T. Masumoto, Mater. Trans. JIM 31 (1990) 747.
[4] Y. He, S.J. Poon, G.J. Shiflet, Science 241 (1988) 1640.
[5] A. Inoue, Prog. Mater. Sci. 43 (1998) 365.
[6] S.J. Hong, T.S. Kim, H.S. Kim, W.T. Kim, B.S. Chun, Mater. Sci. Eng. A 271 (1999) 469.
[7] O.N. Senkov, D.B. Miracle, J.M. Scott, S.V. Senkova, J. Alloys Compd. 365 (2004) 126.
[8] T.S. Kim, S.J. Hong, B.T. Lee, Mater. Sci. Eng. A 363 (2003) 81.
[9] Y.X. Zhuang, J.Z. Jiang, Z.G. Lin, M. Mezouar, W. Crichton, A. Inoue, Appl. Phys. Lett. 79 (2001) 743.
[10] F. Ye, K. Lu, J. Non-Cryst. Solids 262 (2000) 228.
[11] O.N. Senkov, J.M. Scott, D.B. Miracle, J. Alloys Compd. 337 (2002) 83.
[12] P. Si, X. Bian, W. Li, J. Zhang, Z. Yang, Phys. Lett. A 319 (2003) 424.
[13] H.E. Kissinger, Anal. Chem. 29 (1957) 1702.
[14] X.Y. Jiang, Z.C. Zhong, A.L. Greer, Mater. Sci. Eng. A 226–228 (1997) 789.
[15] J.W. Christian, The Theory of Transformations in Metals and Alloys, Pergamon, Oxford, 2002, pp. 529–546.
[16] L.C. Chen, F. Spaepen, J. Appl. Phys. 69 (1991) 679.
[17] L.C. Chen, F. Spaepen, Nature 336 (1988) 366.
[18] A.L. Greer, Acta Metall. 30 (1982) 171.
[19] J.H. Perepezko, R.J. Hebert, R.I. Wu, G. Wilde, J. Non-Cryst. Solids 317 (2003) 52.
[20] T. Gloriant, A.L. Greer, Nanostruct. Mater. 10 (1998) 389.
[21] D.R. Allen, J.C. Foley, J.H. Perepezko, Acta Mater. 46 (1998) 431.